Effects of composition and phonon scattering mechanisms on thermal transport in MFI zeolite films

Yeny Hudiono
School of Chemical & Biomolecular Engineering, Georgia Institute of Technology, Atlanta, Georgia 30332-0100, USA

Abraham Greenstein
Woodruff School of Mechanical Engineering, Georgia Institute of Technology, Atlanta, Georgia 30332-0405, USA

Carine Saha-Kuete
School of Chemical & Biomolecular Engineering, Georgia Institute of Technology, Atlanta, Georgia 30332-0100, USA

Brandon Olson
School of Aerospace and Mechanical Engineering, University of Oklahoma, Norman, Oklahoma 73019-1052, USA

Samuel Graham
Woodruff School of Mechanical Engineering, Georgia Institute of Technology, Atlanta, Georgia 30332-0405, USA

Sankar Nair[a)]
School of Chemical & Biomolecular Engineering, Georgia Institute of Technology, Atlanta, Georgia 30332-0100, USA

(Received 6 June 2007; accepted 16 July 2007; published online 14 September 2007)

We report a systematic study that reveals the effect of composition (silicon-to-aluminum ratio) and the role of different phonon scattering processes on thermal transport in the nanoporous zeolite MFI. This is accomplished via synthesis of a series of films with graded compositions, thermal property measurements, and lattice dynamical modeling in the framework of the Boltzmann equation. MFI films with different Si/Al ratios (from infinity to 26) and constant (*h*0*l*) out-of-plane orientation were successfully synthesized by a seeded hydrothermal process. Three-omega measurements on these films allowed us to obtain comprehensive information on the thermal conductivity of MFI as a function of temperature (150–450 K) and Si/Al ratio. Detailed atomistic simulations (energy minimization and phonon dispersion calculations) were carried out for the MFI crystal structure with different Si/Al ratios and incorporated into a Boltzmann transport model along with approximate theoretical expressions for describing the rate of phonon scattering through umklapp, defect, and boundary scattering processes. The model predicts the observed thermal conductivity behavior very well across the entire range of temperature and composition investigated, with only a small number of fitting parameters of physical significance which allow us to distinguish the contributions of the different phonon scattering mechanisms. In particular, our results strongly suggest that the upper limit of thermal conductivity is defined by boundary-like scattering associated with the pore structure of the material. Below this limit, silicon substitution with aluminum allows considerable suppression of thermal conductivity by point defect scattering and a decrease in phonon velocity. These findings are important from the point of view of developing a robust platform for understanding thermal transport in complex crystalline materials with nanostructural features (such as an ordered nanopore network), which in turn serve as model systems for tuning of phonon transport properties in complex materials. © *2007 American Institute of Physics*.
[DOI: 10.1063/1.2776006]

I. INTRODUCTION

Zeolites are nanoporous mixed-oxide crystals with complex structures formed by corner-sharing oxide tetrahedra (TO_4; T=Si, Al, etc.).[1] There are more than 100 zeolite structures known, as well as a large number of other frameworks obtained by combination with elements favoring octahedral and pentahedral coordination. The capability of altering the composition of a given zeolite (e.g., by lattice atom substitution or by introducing metal cations and organic molecules into the pores) while maintaining the same crystal structure, or conversely the ability to synthesize different crystal structures with the same composition, makes them extraordinarily versatile materials with interesting structure-function relationships[2] as well as many important applications.[3] Newly emerging applications of zeolites include low-*k* di-

[a)]Author to whom correspondence should be addressed. Electronic mail: sankar.nair@chbe.gatech.edu

electric films for computer chips,[4] materials for adsorption cooling devices,[5,6] and hosts for nanotube/wire arrays.[7]

Our interest in the thermal transport properties of zeolite materials originates primarily from their suitability as a model system containing complex, yet well-defined and characterizable, nanostructural features (such as an ordered nanopore network, lattice substitution sites, metal cations or organic species adsorbed in the pores) that interact with heat-carrying phonons, thus offering a number of opportunities for developing and testing models for thermal conductivity in complex crystals. The rich structural complexity of these materials—as well as the increasing significance of thermal transport properties inherent in their emerging applications—justify detailed study of their thermal transport properties, of which current knowledge is relatively limited. There are both experimental difficulties as well as theoretical challenges in describing thermal transport in complex materials with large unit cells.[8–10] The thermal conductivity of zeolites is usually measured by compacting zeolite powders into disks. Computational approaches have relied on classical molecular dynamics simulations, which can provide reasonable property estimates but do not easily allow discrimination of the contributions from several possible phonon scattering mechanisms nor describe well the quantum statistical aspects of the phonon physics. Moreover, there can be large discrepancies[9,11] between measured and computed thermal conductivities.

Here we report our study that combines systematic variation of zeolite composition, measurements of thermal conductivity using well-intergrown polycrystalline zeolite films, and modeling of thermal transport incorporating detailed input from atomistic lattice dynamics calculations (made with a high-quality interatomic potential). This approach allows separation and analysis of the structural and dynamical factors that influence the conductivity. We have chosen the important zeolite MFI (Ref. 8) as a well-characterized model system. MFI has ordered sinusoidal and straight channels of crystallographic pore size ~0.9 nm running along [100] and [010] directions, respectively. It can be made as a pure-SiO_2 material or with different Si/Al ratios (as low as 25). We prepared oriented MFI films of ~10 μm thickness on polished α-alumina substrates by secondary (seeded) growth from a spin-coated seed layer of MFI nanoparticles. The films were polished to sub-10-nm surface roughness and were characterized by x-ray diffraction, scanning probe microscopy, scanning electron microscopy, and energy dispersive spectroscopy to determine the crystal structure, out-of-plane crystal orientation of the film, surface roughness, and Si/Al ratio. We then modeled the thermal conductivity in the framework of the Boltzmann transport equation, with detailed input on phonon dispersion and specific heat from atomistic lattice dynamical simulations. Detailed consideration of various phonon scattering processes, represented by theoretical expressions with a small number of physically significant fitting parameters, allowed us to elucidate both the effects of aluminum incorporation as well as the relative importance of each scattering mechanism, in determining the temperature and composition dependence of the thermal conductivity.

II. EXPERIMENTAL AND COMPUTATIONAL METHODS

A. MFI film synthesis and characterization

Porous α-alumina substrates with porosity of 25% were purchased from Coorstek and polished with SiC paper (Buehler Inc., 400/800 grit) at 140 rpm for 2 min in order to obtain a smooth surface for deposition of MFI nanoparticles. A clear solution with molar ratio of 1 tetraethylorthosilicate (TEOS) (Aldrich): 1 tetrapropylammonium hydroxide (Aldrich): 23 H_2O was hydrothermally reacted at 90 °C for 24 h in a Teflon-lined stainless steel autoclave under rotation, to obtain 100 nm MFI nanoparticles. A 50 wt % MFI nanoparticle dispersion in ethanol was ultrasonicated, filtered and spin-coated (model 100CB, Brewer Science, Inc.) on alumina substrates at 3000 rpm and ramping rate of 500 rpm for 45 s. The coated substrates were placed at an inclined angle (with the seeded side facing downwards) in a Teflon-lined stainless steel autoclave for hydrothermal synthesis at 175 °C (lower Si/Al ratios) for 48 h and 140 °C (higher Si/Al ratios) for 72 h. The secondary growth solutions contained molar ratios of $(4-x)$ TEOS: x Al:0.9 tetrapropylammonium bromide (TPABr) (Aldrich): 0.9 KOH: 940 H_2O, with $0 \leq x \leq 0.25$. The potassium aluminate solution was prepared by hydrolyzing aluminum powder in KOH, TPABr, and water solution for 1 h. The potassium silicate was prepared by mixing TEOS in KOH, TPABr, and water solution for 1 h, and then both solutions were mixed together. The films were rinsed with hot de-ionized water, dried at 60 °C for 3 h, and calcined in air at 500 °C for 6 h with a heating rate of 1 °C/min. The films were then characterized by x-ray diffraction (PANalytical X'Pert Pro, Cu $K\alpha$) to obtain the film orientation. The films were polished with SiC paper (Buehler Inc., 400/800, 600/1200, 1000, and 4000 grit) at 100 rpm for 35 s each. The films were sequentially polished with alumina polishing suspensions of 0.5, 0.3, and 0.05 μm grades. The film roughness was characterized by atomic force microscopy (AFM) (Pico Plus, Molecular Imaging) using the contact mode technique. The film thicknesses and compositions were characterized by a scanning electron microscopy (SEM) (LEO 1550, 10kV) equipped with energy dispersive spectroscopy.

B. Thermal conductivity measurements

The thermal transport properties of MFI zeolite films were characterized using the three-omega technique.[12] A four point probe metal heater was fabricated on the film surface by evaporation of titanium and gold layers through a shadow mask. The thickness of the titanium layer was 30 nm and the thickness of the gold layer was 160 nm. An alternating current signal of amplitude 5 V was applied to the metal heater. Both the in-phase and out-of-phase response of the third harmonic voltage over a frequency range of 75–2000 Hz were employed to analyze the thermal conductivity of the zeolite films. The measurements were performed at temperatures between 150 and 450 K in a vacuum cryostat (~10^{-8} Torr). The three-omega voltage responses were obtained and used to calculate the thermal conductivity. The magnitude and phase of the three-omega voltage are directly related to the temperature response of the metal line, which is a function of

the thermal properties of the underlying material. The thermal conductivity was deduced by a least-squares fit of a two-dimensional analytical solution for a periodic heat source on a multilayer-film-on-substrate system.[12] The thermal conductivity of the substrate was measured separately (see Ref. 13) using the same methods as before. The substrate was shaped into a disk with a thickness of 1 mm and a diameter of 1 in. The specific heat of the porous α-alumina substrate was calculated from the bulk α-alumina heat capacity by first determining the volume fraction of the substrate. This was achieved by physically measuring the mass and the volume of the substrate and comparing to the volume calculated from the density of bulk α-alumina. Then, the heat capacity values of the porous α-alumina were calculated (see Ref. 13) from the known heat capacity of bulk α-alumina. Note that the measurements are made under vacuum, so the porous fraction of the substrate makes no contribution to the specific heat.

C. Energy minimization and phonon dispersion calculations

The dispersion relationships of the MFI zeolites were determined through lattice dynamics modeling. The General Utility Lattice Program[14] was used to minimize the crystal energy, calculate the eigenvalues of the dynamical matrix, and obtain the dispersion relationship along any orientation within the crystal. We used an accurate force field[15] that incorporates coulombic potentials, two-body van der Waals potentials, a three-body interaction term, and furthermore, the polarizability of oxygen through a core-shell treatment. We showed previously[8] that the latter two features are important for accurate specific heat calculations, which can be used to test the quality of the force field. The pure-SiO_2 MFI unit cell has the formula $Si_{96}O_{192}$. To create structures with different Si/Al ratios, random Si atoms were replaced by Al atoms, with the constraint that no two Al sites can be adjacent as dictated by Loewenstein's rule.[16] We used one unit cell [of size ~5.36 nm^3 (Ref. 3) and containing 288 atoms] for the computations, since larger unit cells are computationally too demanding. Aluminum atoms have a charge of +3 whereas silicon atoms have a charge of +4, so every Al substitution requires the addition of a proton to maintain the electrical neutrality of the unit cell. Each proton is placed in a pore and is bonded to an oxygen atom that is bonded to an aluminum atom. The hydrogen atom is placed in the pore, because the interior of the pore is one of the most electronegative regions of the crystal. Furthermore, tetrahedra with aluminum atoms are more electronegative than those with silicon atoms. During the energy minimizations, the fractional coordinates of all the 288 atoms in the MFI structure are allowed to relax and the unit cell parameters are left constant at the values obtained from the crystal structure.[1] Newton–Raphson and rational function optimization minimization techniques are used. The potential energy surface is complicated and has many saddle points. Therefore, care must be taken when analyzing the results. The eigenfrequencies reveal if a local minimum has been reached. If all the phonons frequencies are real the dynamical matrix is positive definite, which implies the positive definiteness of the Hessian matrix. The structures are also examined visually to verify their reasonableness. The full anisotropic phonon dispersions for all 864 branches were then calculated across the entire Brillouin zone. The dispersions are calculated by evaluating the square roots of the dynamical matrix eigenvalues across an evenly spaced grid of 1000 points that spans the positive octant of the Brillouin zone. The effect of aluminum configurations is checked by calculating the dispersion for two structures with the same Si/Al ratios but different aluminum atom locations. The resulting dispersions are only weakly dependent on the configuration of the aluminum atoms. See Ref. 13 for sample results of the phonon dispersion and phonon speed for one branch. Similar calculations are done for all 864 branches.

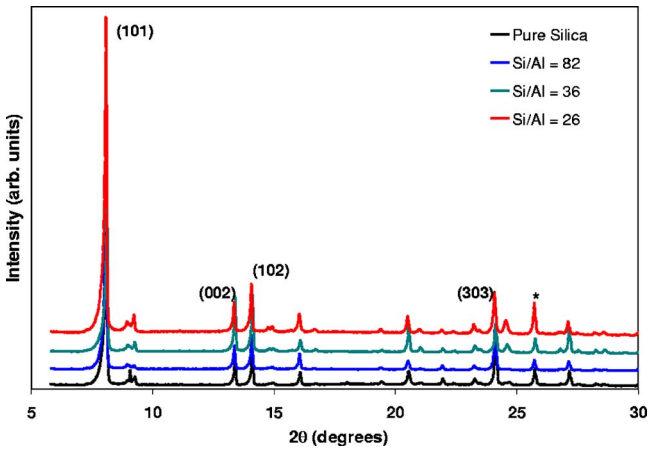

FIG. 1. X-ray diffraction patterns of MFI films as a function of composition, showing the high degree of ($h0l$) out-of-plane orientation (* represents the peak from the alumina substrate).

III. RESULTS AND DISCUSSION

The introduction of aluminum into the synthesis changes the crystal growth characteristics (and thus the film orientation) in ways that are poorly understood. Considerable optimization of the synthesis conditions (temperature, composition) was necessary to synthesize several MFI films with varying Si/Al ratios, all with the same ($h0l$) out-of-plane orientation as shown by x-ray diffraction (Fig. 1). MFI films with Si/Al ratios below 25 could not be prepared irrespective of the crystal orientation, for reasons that are likely related to the stability of the crystal structure and the alteration of the growth mechanism in the presence of larger amounts of aluminum precursors. Figure 2 shows the SEM top views of a

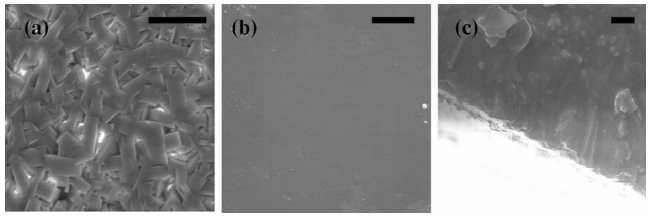

FIG. 2. SEM images of MFI films: (a) top view of MFI films, (b) polished surface of MFI films, and (c) cross-sectional view of MFI films. Scale bars are 10, 5, and 1 μm, respectively.

TABLE I. MFI film composition (measured by EDS), and rms roughness (measured by AFM). Sample 1 has an Al content below the least count of EDS.

No.	Si/Al ratio in synthesis composition	Growth T(°C)	Actual Si/Al ratio	rms roughness (Å)	Scherrer domain size (nm)
1	∞	140	>400	102±10	97±2
2	100	140	82±15	65±10	100±2
3	65	175	36±6	64±10	94±2
4	35	175	26±5	45±10	93±2

typical film before and after polishing, and the cross-section view of the film after polishing. The polishing step was found to be important for reliable heater deposition prior to three-omega measurements of thermal conductivity. Table I summarizes the obtained Si/Al ratios from energy dispersive spectroscopy (EDS), the root-mean-square (rms) roughnesses from AFM, and the Scherrer domain sizes (*vide infra*) obtained from x-ray diffraction (XRD). The EDS results were obtained using an electron beam of 3 μm spot size and were averaged over numerous regions of the membrane cross section to obtain a reliable estimate of the composition. The present MFI films are measured to have Si/Al ratios of ∞, 82, 36, and 26. Figure 3 shows the thermal conductivity of $(h0l)$-oriented MFI films as a function of Si/Al ratio in the temperature range of 150–450 K. It is clear that the thermal conductivity varies continuously as a function of the aluminum content. Furthermore, the conductivity increases with temperature over the entire range investigated. It was verified through repeated experimentation that the observed behavior was not the result of artifacts arising, e.g., from heater contact resistance.

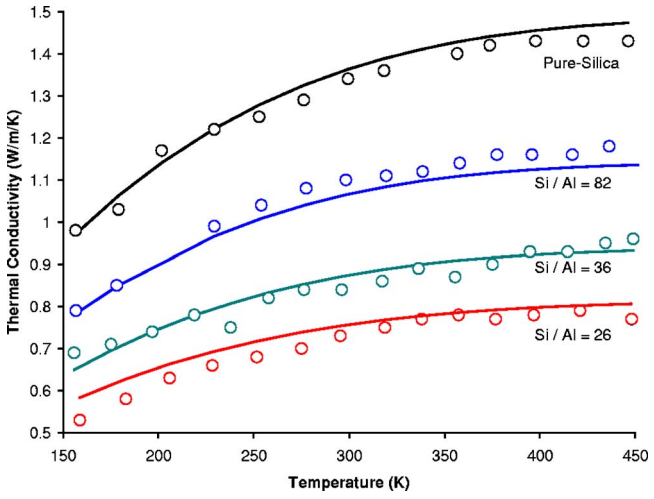

FIG. 3. Measured thermal conductivity of MFI films as a function of Si/Al ratio over a temperature range of 150–450 K. Symbols are experimental data and solid lines are model predictions. Experimental error estimate is approximately 0.01 W/m/K.

The observed thermal conductivity could not be explained by previous models[8,10,11,17] which assume that the acoustic phonon dispersions can be treated as linear and isotropic, and that the optical modes can be neglected. We were able to successfully model the thermal conductivity with a considerably more detailed approach. Crystal structures with Si/Al ratios of 95, 47, and 31 were created and used to describe the behavior of the experimentally generated Si/Al ratios of 82, 36, and 26. This approximation is made in an obviously consistent manner and does not lead to any loss of understanding of the phonon physics. Examples of the calculated phonon dispersion curves are shown in Ref. 13. The expression used to calculate conductivity in any crystal direction j is

$$k_j = \frac{k_b}{8\pi^3}\sum_P \int\int\int \left(\frac{\hbar\omega}{k_bT}\right)^2 \times \frac{e^{\hbar\omega/k_bT}}{(e^{\hbar\omega/k_bT}-1)^2} v_j^2 \tau_j(\omega) dK_x dK_y dK_z. \quad (1)$$

The integral is over a discretized grid throughout the entire Brillouin zone and the summation is over all polarizations. The phonon velocity v_j is the local gradient of the dispersion projected onto crystallographic direction j, in this case [101] which is the primary out-of-plane orientation of the polycrystalline film. The phonon velocities are calculated for every phonon branch at every point of the computational grid in the Brillouin zone, using the previously calculated phonon dispersion curves. The dispersion curves are also used to calculate the phonon specific heat contribution to the thermal conductivity, as represented by the first two terms in the integral of Eq. (1).

A critical issue in modeling thermal conductivity of crystals is the calculation of the phonon relaxation lifetimes that are a consequence of different phonon scattering mechanisms operating in the material. In theory, the relaxation time τ_j can be calculated from the Fermi scattering equation.[17] However, this calculation is extremely expensive for a simple material, and all but impossible for a complex material such as MFI. Some components of τ_j can be estimated from molecular dynamics,[9] but defect and boundary scattering cannot be easily accounted for. There have also been molecular dynamics studies that explicitly calculate phonon lifetimes in simple crystals,[18,19] but this approach requires a large number of simulations with varying system sizes in order to adequately sample the Brillouin zone. The size and

complexity of the MFI unit cell precludes the computational feasibility of this approach. As a result, semitheoretical expressions are used to estimate the relaxation times.[8–11,17] The three processes considered in the present conductivity model are umklapp (U) phonon-phonon scattering, boundary scattering, and point defect scattering. It was shown[20] that normal (N) phonon-phonon scattering is unimportant in quartz, and the same is assumed in MFI. The expression used for U processes is[17]

$$\tau_U^{-1} = B\omega^2 T e^{-\theta/3T}. \tag{2}$$

Here, θ is the Debye temperature and is estimated to be 926 K for MFI. This estimate is obtained by fitting the Debye model of specific heat to experimental data.[8] However, the calculated results are insensitive to the exact value of the Debye temperature used, for reasons that will become clear during the subsequent analysis of relaxation time behavior. As temperature increases, U processes dominate and the conductivity would become inversely proportional to temperature. This semitheoretical expression is the least rigorous part of the model but is still capable of providing a semiquantitative estimate of the importance of this phonon scattering mechanism in determining the thermal properties. Point defect scattering occurs from isolated zero-dimensional defects, while boundary scattering occurs from two dimensional planar defects (such as grain boundaries, stacking faults, or lattice-strained planes) that divide the crystal into domains. The expression for point defect scattering is[17]

$$\tau_D^{-1} = A\omega^2 g(\omega). \tag{3}$$

Here $g(\omega)$ is the phonon density of states. In principle, the material-dependent constant A can be calculated "*ab initio*," but in practice this requires far more structural information about the defects than is practical to ascertain. Therefore, A is treated as a fitted parameter, which can now be reliably determined because of the existence of a series of samples with varying numbers of point defects. The expression for boundary scattering is[17]

$$\tau_B^{-1} = v/l_{\text{eff}}. \tag{4}$$

The effective distance a phonon travels between boundary scattering events could be estimated theoretically if enough information about the domains (shape, size, interfacial reflectivity) were available. Since it is not practical to obtain this information, the effective distance is also treated as a fitted constant. The overall inverse relaxation time is calculated by summing the inverse relaxation time contributions from Eqs. (2)–(4). Then Eq. (1) is used to fit the model by nonlinear least squares to the experimental data. Note that there are only three parameters in the fit: A, B, and l_{eff}, of which the last two are constant across all the samples. We ensured that a large parameter space was explored by using a number of initial guesses. A unique best-fit result of high quality was obtained as shown in Fig. 3 and the fitted parameters are summarized in Table II. The parameter A depends nonlinearly on the Si/Al ratio, since Al atoms can influence phonon transport by scattering from an impurity atom of different mass, difference in the effective spring constant of Al-O bonds, and local strain fields that scatter phonons.

TABLE II. Fitted phonon scattering model parameters for MFI films. Umklapp parameter B and effective domain size l_{eff} are held constant across all the samples whereas A varies with Al content.

Si/Al ratio	A (10^{-31} s/rad^2)	B (10^{-21} s/K rad^2)	l_{eff} (nm)
∞	5.7±0.1	7.4±0.1	4.8±0.1
82	6.4±0.1	7.4±0.1	4.8±0.1
36	45.2±0.1	7.4±0.1	4.8±0.1
26	85.2±0.1	7.4±0.1	4.8±0.1

Despite the inclusion of U processes, the thermal conductivity of MFI increases with temperature, implying that other scattering processes as well as specific heat effects dominate the temperature dependence. We found that the boundary scattering term (with a fitted l_{eff} of 4.8 nm) makes by far the strongest contribution of the three phonon scattering mechanisms and limits the absolute value of the thermal conductivity. The obtained value of l_{eff} is worthy of more detailed discussion. Several authors report the existence of sub-100-nm domains in zeolite crystals.[21,22] An upper limit on the domain size is estimated from XRD as ~100 nm (Table I) by the Scherrer relation[23] which uses the full width at half maximum of the XRD peaks. However, the Scherrer domain size (~100 nm) is much larger than the fitted l_{eff} and is unlikely to limit the propagation of phonons at nanometer length scales. Furthermore, the MFI structure is inherently free of pore stacking faults[1,24] that might also act as phonon scattering boundaries. The high quality of the obtained fit strongly implies that the temperature-independent boundary-like scattering mechanism arises from the interaction of the lattice vibrations with the pore network, which disrupts long-range lattice vibrations. The periodicity of the pore structure in MFI is about 1.5 nm and the crystallographic pore size is about 0.9 nm.[24] Heat carriers would thus have a mean free path that is determined by the length scale of the pore network. From the point of view of real-space visualization of thermal transport (as opposed to the present reciprocal-space approach), the presence of nanoscale voids would impede the atom-to-atom transfer of heat energy at the surfaces of these voids, since this heat energy must be either reflected back from the void/pore or be channeled around it. Very recently, similar arguments (based upon the results of molecular dynamics simulations) have been advanced to qualitatively explain the thermal conductivity of nanoporous metal-organic frameworks.[25] The temperature-independence of the main phonon scattering mechanism in MFI also explains the unusual (viz. monotonically increasing) temperature dependence of the conductivity, which is well described by the increase in specific heat with increasing temperature (also see Fig. 4 and the following discussion). We note that the umklapp relaxation time expression [Eq. (2)] is the most rigorous one available from previous theoretical efforts, but is still based on assumptions that may not be perfectly valid for MFI. Future work could focus on developing a general umklapp term valid for all phonon branches, which could then allow a more quantitatively accurate estimate of the relative importance of boundary and umklapp effects on phonon transport in complex crystals.

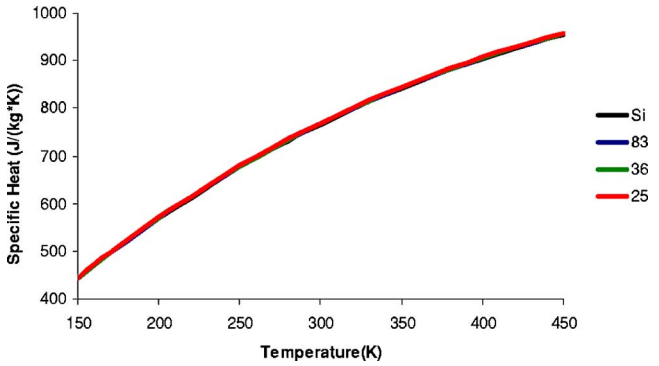

FIG. 4. Calculated specific heat of MFI for different Si/Al ratios. All curves overlap and the differences are negligible.

Below the upper limit defined by boundary scattering, Al incorporation can effectively suppress the conductivity as seen from the rapid increase in the value of the parameter A with increasing Al content. Our approach allows us to determine whether this is due to decreased specific heat, decreased phonon velocity, or increased point defect scattering. The calculated specific heat (Fig. 4) changes negligibly with increasing Al content, whereas the mean phonon velocity [Figs. 5(a) and 5(b)] changes significantly. These results may seem surprising because both quantities are calculated directly from the dispersion curves. However, the modal specific heats are fairly insensitive to small/moderate amounts of Al because states with energies much lower than k_bT all have the same specific heat and states with energies much higher than k_bT do not contribute as much to the specific heat. The mean phonon velocity is calculated by taking a weighted average of the modal velocities of all phonon states. It is calculated with both the modal specific heat and the modal thermal conductivity as weighting functions [Figs. 5(a) and 5(b), respectively]. The specific-heat-weighted mean phonon velocity decreases significantly with increasing aluminum content because aluminum has a smaller charge than silicon, so the aluminum-oxygen bond is softer than the silicon-oxygen bond. The average speed decreases with increasing temperature, because phonon branches with higher frequencies start contributing to the specific heat and these phonon branches tend to have smaller group velocities. When modal conductivity is used as a weighting function, one obtains a more accurate estimate of the group velocities of phonons that contribute to thermal conduction. However, this method also makes it difficult to discern whether the mean phonon velocity is changing because different scattering mechanisms affect the distribution of heat over different phonon states, or whether the phonons are actually slowing. The conductivity-weighted mean phonon speed starts to increase at higher temperatures because the umklapp scattering term becomes stronger and it scatters high-frequency, low-velocity phonons more strongly than the faster lower-frequency phonons. Irrespective of the weighting method, the results of Fig. 5 show that the presence of Al atoms slow the mean phonon velocity by about 25% from pure-silica MFI to the sample with Si/Al=26. However, the observed decrease in thermal conductivity (Fig. 3) is also due to increased point defect scattering. We note from Table II that

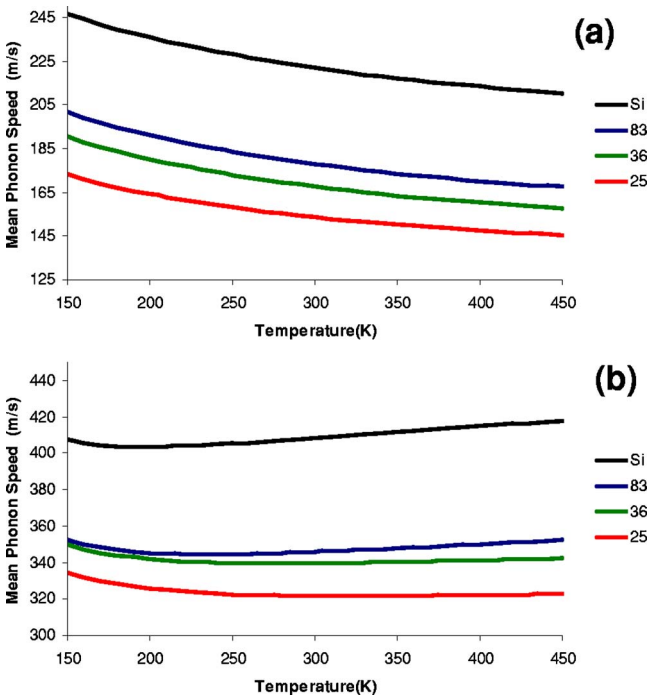

FIG. 5. Calculated mean phonon speeds in MFI for the (101) direction and different Si/Al ratios with (a) the modal specific heat as weighting function and (b) the modal thermal conductivity as weighting function.

the point defect scattering parameter A is negligible for the pure-SiO_2 sample (but not zero since there is still a small concentration of defects such as missing Si atoms),[1] and that it increases sharply with Al content to an extent that defect scattering makes a significant contribution to the drop in conductivity at higher Al contents. It is important to mention that the effect of Al incorporation is stronger than that expected simply from the "isotope" effect (i.e., substitution of Si with Al, which has a slightly different atomic mass). The Al-O bonds are softer than the Si-O bonds and the resulting local strain would significantly impede the transfer of heat energy (i.e., serve as localized phonon scatterers in reciprocal space) in addition to slowing the mean phonon velocity. This phenomenon has also been visualized in real-space for other aluminosilicate materials by molecular dynamics simulations.[9]

IV. CONCLUSION

We have presented a combined experimental, computational, and theoretical approach that leads to some new findings regarding the mechanisms of phonon transport in nanoporous materials. Using a controlled hydrothermal zeolite thin film growth technique, we were able to prepare a series of MFI films with constant out-of-plane orientation and different Si/Al ratios. Combining three-omega measurements with energy-dispersive x-ray analysis of the film composition, we obtained a first set of comprehensive data on thermal transport in MFI as a function of temperature and composition. The developed model, which incorporates information from detailed atomistic lattice dynamics calculations, well describes the observed behavior and strongly suggests that the main phonon scattering mechanism limiting the

thermal conductivity of nanoporous crystals such as MFI is the boundary-like scattering from the pore network. We also find that Al incorporation significantly suppresses the thermal conductivity due to a combination of phonon slowing and localized phonon scattering, and not due to specific heat or isotope scattering effects. It is important to emphasize that the present approach, although approximate in the handling of phonon scattering, still represents a considerable advance in measuring and modeling the thermal conductivity of zeolite materials. The synthesis of polycrystalline thin films with controlled compositional variation, thermal property measurements on these films, and the current modeling approach together have potential as a robust platform for understanding thermal transport in complex crystals and separating the contributions from different scattering processes. The important roles of boundary and defect scattering, as illustrated here, also imply that the thermal conductivity of these complex crystals can be tuned by exploiting not only the composition but also the pore structure, e.g., by the inclusion of molecular species in the pores.

ACKNOWLEDGMENTS

The authors acknowledge partial support of this work by NSF (CTS-0437621, CAREER CTS-044879) and Georgia Tech. They also acknowledge A. G. Ahmadi for assistance with heater deposition.

[1]C. Baerlocher, W. M. Meier, and D. H. Olson, *Atlas of Zeolite Framework Types*, 5th ed. (Elsevier, Amsterdam, 2001).
[2]M. E. Davis, Nature (London) **417**, 813 (2002).
[3]M. Tsapatsis, AIChE J. **48**, 654 (2002).
[4]Z. J. Li, M. C. Johnson, M. W. Sun, E. T. Ryan, D. J. Earl, W. Maichen, J. I. Martin, S. Li, C. M. Lew, J. Wang, M. W. Deem, M. E. Davis, and Y. S. Yan, Angew. Chem. Int. Ed. **45**, 6329 (2006).
[5]X. L. Wang, H. T. Chua, and K. C. Ng, Int. J.Refrig. **28**, 756 (2005).
[6]J. M. Gordon, K. C. Ng, H. T. Chua, and A. Chakraborty, Int. J.Refrig. **25**, 1025 (2002).
[7]K. Mukhopadhyay, A. Koshio, N. Tanaka, and H. Shinohara, Jpn. J. Appl. Phys., Part 2 **37**, L1257 (1998).
[8]A. M. Greenstein, S. Graham, Y. C. Hudiono, and S. Nair, Nanoscale and Microscale Thermophysical Engineering **10**, 321 (2006).
[9]A. J. H. McGaughey and M. Kaviany, Int. J. Heat Mass Transfer **47**, 1799 (2004).
[10]V. V. Murashov, J. Phys.: Condens. Matter **11**, 1261 (1999).
[11]V. V. Murashov and M. A. White, Mater. Chem. Phys. **75**, 178 (2002).
[12]B. Olson, S. Graham, and K. Chen, Rev. Sci. Instrum. **76**, 053901(2005).
[13]See EPAPS Document No. E-JAPIAU-102-060717 for further details of experimental methods, results of phonon dispersion calculations, and fitted parameter values. This document can be reached via a direct link in the online article's HTML reference section or via the EPAPS homepage (http://www.aip.org/pubservs/epaps.html_).
[14]J. D. Gale, J. Chem. Soc., Faraday Trans. **93**, 629 (1997).
[15]M. J. Sanders, M. Leslie, and C. R. A. Catlow, J. Chem. Soc. Chem. Commun. **19**, 1271 (1984).
[16]A. J. Vega, J. Phys. Chem. **100**, 833 (1996).
[17]G. P. Srivastava, *The Physics of Phonons* (Adam Hilger, Bristol, UK, 1990).
[18]A. J. C. Ladd, B. Moran, and W. G. Hoover, Phys. Rev. B **34**, 5058 (1986).
[19]A. J. H. McGaughey and M. Kaviany, Phys. Rev. B **69**, 094303 (2004).
[20]P. G. Klemens, Proc. R. Soc. London, Ser. A **208**, 108 (1951).
[21]T. M. Davis, T. O. Drews, H. Ramanan, C. He, J. S. Dong, H. Schnablegger, M. A. Katsoulakis, E. Kokkoli, A. V. McCormick, R. L. Penn, and M. Tsapatsis, Nat. Mater. **5**, 400 (2006).
[22]G. González, W. Stracke, Z. Lopez, U. Keller, A. Ricker, and R. Reichelt, Microsc. Microanal. **10**, 224 (2004).
[23]Z. Kaszkur, Z. Kristallogr. **23**, 147 (2006).
[24]H. van Koningsveld, J. C. Jansen, and H. van Bekkum, Zeolites **10**, 235 (1990).
[25]B. L. Huang, A. J. H. McGaughey, and M. Kaviany, Int. J. Heat Mass Transfer **50**, 393 (2007).